Pergamon

PII: S0191-8141(97)00096-5

Journal of Structural Geology, Vol. 20, No. 4, pp. 407 to 416, 1998

0191-8141/98 $19.00 + 0.00

Material transfer in accretionary wedges from analysis of a systematic series of analog experiments

MARC-ANDRÉ GUTSCHER and NINA KUKOWSKI

GEOMAR, University Kiel, Wischhofstrasse 1-3, D-24148, Kiel, Germany

and

JACQUES MALAVIEILLE and SERGE LALLEMAND

Lab. de Géophysique et Tectonique, Université de Montpellier II, UMR 5573, CNRS, Montpellier, France

(*Received* 28 *October* 1996; *accepted in revised form* 6 *October* 1997)

Abstract—The structural evolution of accretionary wedges was modeled in a series of analog experiments with systematically varying initial boundary conditions. The two principle parameters investigated were basal friction and thickness of sediment **I**nput (relative to subducted sediment **O**utput). Material transfer (in terms of degree and location of accretion and erosion) is quantified as a function of these two parameters. Low basal friction produces long, thin wedges, by continuous frontal accretion of imbricate thrusts. Simultaneously, substantial basal erosion may occur, with little influence on the frontal dynamics. The formation of an outer arc high with an accompanying forearc basin depends upon the relative amount of basal erosion, the opening of the subduction window. Spacing of thrust faults is proportional to the layer thickness confirming the principle of self-similar wedge growth from critical wedge theory. High basal friction typically generates steep wedges, marked by an erosional, mass wasting frontal slope in the cases $\mathbf{I} \leq \mathbf{O}$. This is due to underthrusting and/or subduction of the entire sedimentary section. The case $\mathbf{I} < \mathbf{O}$ also features the late development of normal faulting and an extensional forearc basin.

For both low and high basal friction the material balance affects the wedge slope; erosive conditions ($\mathbf{I} < \mathbf{O}$) lead to steeper wedges than accretionary conditions ($\mathbf{I} > \mathbf{O}$). For low basal friction the primary modes of material transfer are frontal accretion and basal erosion. For high basal friction the primary modes of material transfer are underthrusting/underplating and frontal erosion. Applying the experimental results to active convergent margins, parallels may be drawn. Thus, the Barbados Ridge Complex is interpreted to be a good example of a low basal friction wedge with an accretionary material balance, while the Japan and Mariana margins provide examples of an erosive material balance.

INTRODUCTION

The Earth's convergent margins are the sites of large scale material flux (1–2 km^3/year) between the oceanic and continental lithospheres, the asthenosphere and atmosphere (von Huene and Scholl, 1991). Ninety per cent of the global seismic moment release occurs in the shallow regions (< 50 km) of subduction zones (Pacheco *et al.*, 1993). Whereas some convergent margins are marked by a broad (30–100 + km) accretionary wedge (e.g. Alaska, Makran, S. Barbados Ridge), those accumulated as sediments are scraped off the downgoing oceanic plate, others (e.g. Marianas, Tonga, N. Chile, Japan) have only a steep and narrow wedge and are currently erosional (Hussong and Uyeda, 1982; Lallemand *et al.*, 1994). Geological evidence, in the form of major unconformities, subsidence of the margin and landward migration of the volcanic arc, suggests that some margins have retreated at rates of up to 3 km/Ma during the past 20 Ma (von Huene and Lallemand, 1990).

Seismic reflection profiling has recorded structural information in submarine accretionary wedges down to depths of 10 km (Westbrook *et al.*, 1988; Moore *et al.*, 1990, 1991; Shipley *et al.*, 1992), while bathymetric images of the surface morphology (Hussong *et al.*, 1988; Davis *et al.*, 1990; von Huene *et al.*, 1995) add a third dimension to the structures observed. Deep Sea Drilling Project (DSDP) and Ocean Drilling Program (ODP) drilling has corroborated the presence of frontal folds and thrusts, with steeply dipping and overturned beds, and at two convergent margins, has penetrated the basal detachment (Taira *et al.*, 1992; Moore *et al.*, 1995). In most cases, however, these data only provide good structural control in the uppermost 1–2 km, because seismic image quality deteriorates with increasing depth. Furthermore, these data represent a snapshot in time. In order to better understand the structural evolution of accretionary wedges, forward deformation models are necessary.

Early tectonic models of accretionary wedges featured offscraping of the entire sedimentary section as a series of imbricate thrust slices (Dickinson and Seely, 1979). Later models included a layer of subducting material dragged along with the downgoing plate, possibly causing basal or 'tectonic' erosion (Scholl *et al.*, 1980). Theoretical mechanical models (Davis *et al.*, 1983; Dahlen, 1984) compare a submarine accretionary wedge to a growing pile of soil or snow, deforming in front of a bulldozer.

Both are considered to be 'critical wedges', internally on the verge of failure throughout, and whose geometry is defined by the material strength and strength of the basal detachment. This so called critical wedge theory predicts that deformation in accretionary wedges (with negligible cohesion) is scale independent (i.e. that wedge growth is self-similar) and has formed the basis for numerous analog modeling investigations using granular materials. This forward modeling technique demonstrated a similarity between deformation in model wedges and structures observed in fold-and-thrust belts and/or submarine accretionary wedges (Davis *et al.*, 1983; Malavieille, 1984). Subsequent investigations indicated the importance of certain parameters such as basal friction, layer thickness and relative strength of the backstop material (Mulugeta, 1988; Byrne *et al.*, 1988; Malavieile *et al.*, 1991; Liu *et al.*, 1992; Lallemand *et al.*, 1994).

Since seismic reflection profiles (Westbrook *et al.*, 1982; Moore *et al.*, 1990), isotopic signatures in arc melts (Morris *et al.*, 1990; Leeman *et al.*, 1994) and mass balance calculations (von Huene and Scholl, 1991; von Huene *et al.*, 1996) all provide evidence that a layer of sediment is subducted beneath the backstop and into the mantle, this feature was incorporated into experimental models (Lallemand, 1992a,b; Kukowski *et al.*, 1994). The presence of material output demonstrated that basal erosion can occur simultaneously with frontal accretion (Kukowski *et al.*, 1994). These studies suggested a need to quantify the influence of basal friction and relative sediment input on the evolution and material transfer in thrust wedges.

OBJECTIVES

This study investigates the structural evolution in the shallow portions (< 10 km depth) of accretionary wedges through analog modeling. The goal is to determine how two fundamental parameters (basal friction, ratio of sediment input to output) govern the material transfer. Material transfer is expressed by four tectonic processes; (1) frontal accretion, (2) frontal erosion, (3) basal accretion (or underplating), and (4) basal erosion. A further goal is to determine under which conditions several processes may occur simultaneously and if evolution is progressive or episodic.

EXPERIMENTAL SETUP AND VARIATION OF PARAMETERS

To achieve the set goals a systematic series of analog experiments was performed where the two initial parameters were varied, to test their influence on the tectonic evolution. All experiments reported here were performed at the Laboratoire de Tectonique of the University of Montpellier, France. The apparatus consists of a 240 cm long, 30 cm wide and 60 cm high glass sided box, with a

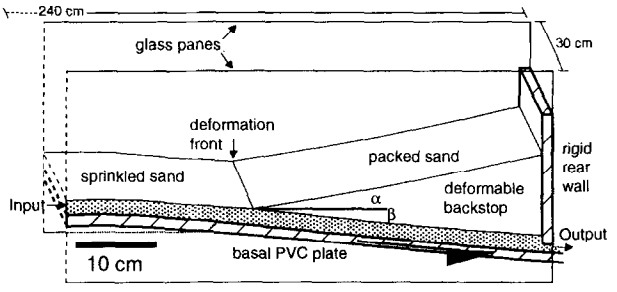

Fig. 1. Three-dimensional perspective view of the experimental apparatus. The basal PVC plate can be treated to produce different basal frictions. Sprinkled sand (**Input**) represents undeformed deep sea sediments and a deformable backstop composed of packed sand is placed against the vertical rear wall. An opening at the base of the wall (the 'subduction window') can be opened to the desired aperture, allowing material to exit the system (**Output**).

basal PVC plate, treated to obtain different basal frictions and curved to the desired geometry (Malavieille, 1984; Lallemand *et al.*, 1994) (Fig. 1). Well sorted eolian quartz sand, diameter 0.3–0.5 mm, with an internal coefficient of friction of 0.6, is chosen as an analog material because it exhibits a depth-dependent Coulomb rheology, most appropriate for investigations of upper crustal rocks and marine sediments.

The layer of sprinkled sand on the basal plate is termed '**Input**' and represents the deep sea sediments and trench fill overlying the subducting oceanic plate. The basal plate is pulled by a motor to simulate subduction of the oceanic plate. The rigid rear wall can be raised or lowered, creating an opening (also termed 'subduction window'), typically 0–2 cm in size. This allows a known amount of material to leave the system (termed '**Output**'), which represents the subducted sediment transported beyond the frontal portion of the wedge. An initial wedge of deformable material (packed sand or more cohesive material) is placed against the rear wall, overlying the sprinkled sand and serves as a deformable backstop. This represents the more competent metamorphosed sediments or crystalline crust (backstop) in convergent margins, against which unconsolidated sediments are offscraped (Byrne *et al.*, 1993). Passive colored marker horizons allow observation of deformation throughout an experiment, through the lateral glass panes. Edge effects are minimized through application of a low friction polymer coating to the glass panes. The final stage can be moistened and sectioned to examine the internal structure and control the degree of edge effects. These were negligible in the experiments reported here.

For the scaling factor of 10^{-5} used in these experiments, 1 cm in the model scales to 1 km of upper crustal rocks. Thus, the cohesion of the sprinkled sand (≈ 20 Pa) and the cohesion of the packed sand, (≈ 100 Pa) and packed mortar (≈ 150 Pa) backstops used, scale, respectively, to 2, 10 and 15 MPa, which in each case are reasonable values for unconsolidated marine sediments and lithified sedimentary rocks (Hoshino *et al.*, 1972).

The physical parameters (coefficient of friction, cohesion) of the analog materials (sand, dry mortar, etc.) and basal surfaces were measured in the laboratory using a motor driven shear box apparatus including a stress meter. This provides more accurate results than simple shear box devices, only capable of measuring maximum yield stress (Krantz, 1991).

A core series of six analog experiments forms a matrix where two basic parameters, basal friction and ratio of Input to Output (**I/O**), are varied systematically. These experiments all share a similar initial geometry, yet produced a variety of final configurations (Fig. 2a). This core series was expanded to 12 experiments to cover a broader range of Input to Output ratios and allow a quantitative analysis of material transfer. In general, low basal friction produced long, thin wedges, while high basal friction led to shorter, steeper wedges, for otherwise similar conditions.

Based on critical wedge theory, the basal friction and internal strength of the analog material define a taper stability field, within which a wedge can increase or diminish in size (Dahlen, 1984). Above this field, the material is subject to extensional failure at the oversteepened front where slumps and slides occur. Below this field, the compressive stress exceeds the shear strength along a decollement and a new basal and frontal thrust fault develops, thickening the front of the pile. The range of surface slopes observed during the course of the six matrix experiments is displayed in the stability field diagram for the experimental sand (Fig. 2b). In most experiments, a wide range of surface slopes is observed. Low basal friction experiment N4, (with a positive, 'accretionary' mass balance) remains at the lower boundary of the stability field throughout the entire experiment. Similarly, all low basal friction experiments with excess material input remain at the lower boundary of the stability field, maintaining a 'critical taper' in accordance to critical wedge theory (Davis *et al.*, 1983). In general, erosional conditions lead to steeper final wedge configurations (Fig. 2).

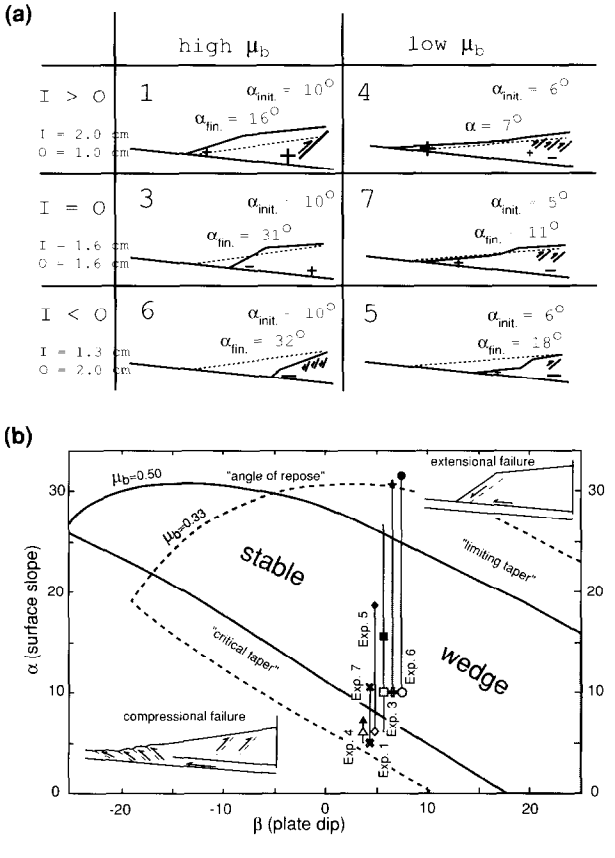

Fig. 2. (a) Matrix of six key experiments, with initial geometry (dashed lines and index 'init.') and final geometry (solid lines and index 'fin.'), '+' represents local accretion, '−' represents local erosion (symbols scaled according to degree). Backthrusts and normal faults are shown schematically. (b) Taper stability field for the experimental sand with paths taken by the six key experiments, initial and final geometry (open and closed symbols, respectively), solid boundaries and shaded region for high basal friction, dashed for low basal friction.

EXPERIMENTAL RESULTS

Before the material transfer from the entire series of experiments is reported, the tectonic evolution and specific features (i.e. morphology, material transfer, fault spacing) of low basal friction experiments will be described in detail and compared briefly to high basal friction experiments. Since a thorough discussion of the latter is given elsewhere (Gutscher *et al.*, 1996; Gutscher *et al.*, in press), only two examples will be presented here in order to illustrate the deformation processes (i.e. underthrusting, frontal erosion) unique to high basal friction experiments.

The tectonic interpretation of low basal friction experiment (N0) with zero Output is presented first as a reference experiment (Fig. 3). Here all the material on the subducting plate is offscraped and the wedge grows in self-similar fashion. The offscraped material is accreted frontally as a series of regularly spaced imbricate thrust slices. The frontal slope of the wedge remains constant at ca. 6° (the critical taper), in agreement with critical wedge theory (Davis *et al.*, 1983). Backthrusting at the apex of the initial wedge builds a substantial outer arc high which bounds a potential forearc basin arcwards. This depression would fill to form a true forearc basin if sedimentation were simulated (Malavieille *et al.*, 1993; Larroque *et al.*, 1995; Wang and Davis, 1996). Wedge evolution can be described as progressive, steady state growth, with the overall geometry similar at all stages.

In contrast, in low basal friction experiment N7, material Input equals material Output, and thus the total wedge experiences no net growth (Fig. 4). Nevertheless, a series of regularly spaced imbricate thrust slices develop at the front. Simultaneously, substantial erosion occurs as an out-of-sequence thrust cuts through the backstop, eroding its base and creating a scarp where it emerges at the mid-slope. Wedge evolution is not progressive but transient, marked by separate stages.

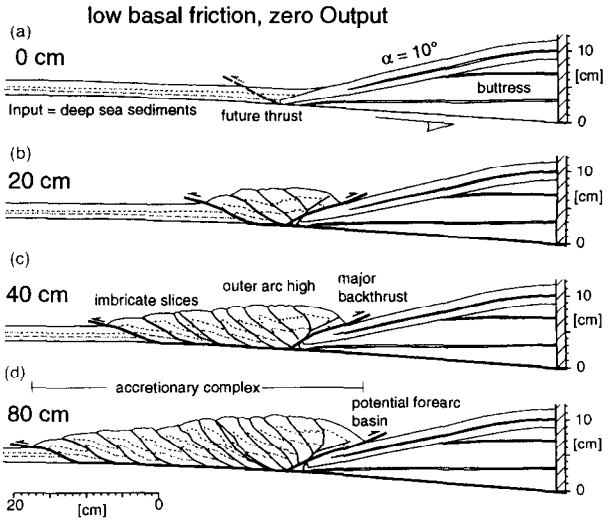

Fig. 3. Tectonic interpretation of experiment N0, low basal friction, Input = 2.0 cm, Output ≤ 0.1 cm, $\alpha = 10°$, $\beta = 5°$. (a) 0 cm (b) 20 cm (c) 40 cm (d) 80 cm convergence.

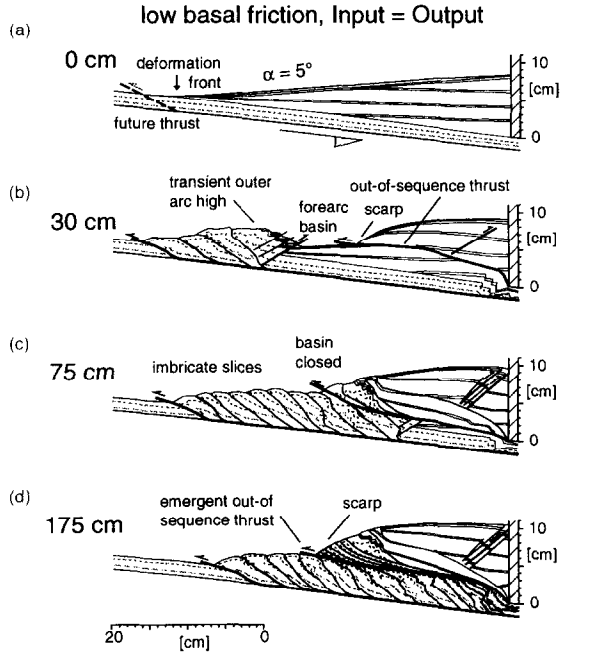

Fig. 4. Tectonic interpretation of experiment N7, low basal friction, Input = 1.6 cm, Output = 1.6 cm, $\alpha = 5°$, $\beta = 5°$. (a) 0 cm (b) 30 cm (c) 75 cm (d) 175 cm convergence.

First an outer arc high and forearc basin are formed. These transient features are then destroyed by motion along the out-of-sequence thrust (Fig. 4b,c). During the last stage, imbricate slices formed at the front are entrained beneath the backstop becoming duplexes and are subsequently subducted (Fig. 4c,d). The frontal region of imbricate slices has a shallow surface slope (ca. 6–10°) in agreement with critical wedge theory, but the mid-slope is steeper (ca. 20–30°) due to the emergent out-of-sequence thrust.

This pattern of simultaneous frontal accretion and basal erosion, with a shallow frontal slope and steeper mid-slope, is observed in all low basal friction experiments with an open subduction window. Net growth or net erosion depends on the material balance (amount of Input relative to Output). For a positive or 'accretionary' material balance with an open subduction window (i.e. experiment N4—Fig. 5b), the configuration is intermediate between experiments N0 and N7 (see also Gutscher *et al.*, 1996—fig. 3b).

New thrust faults in low basal friction experiments are observed to develop at regular and relatively short intervals. The average fault spacing was found to be proportional to layer thickness. This is shown in photographs of three experiments (Fig. 5) with different layer thicknesses after the same amount of scaled convergence (20 × layer thickness). The Input layer thicknesses are 1.0, 2.0 and 3.3 cm, respectively, and after the same relative amount of convergence (i.e. 20, 40 and 65 cm), a comparable number of thrust slices (6–8) have formed in all three cases. Two additional variables, the initial wedge configuration (α) and backstop material exerted only a negligible effect on low basal friction experiments. Initial surface slopes of 5–15° were tested and had no effect on fault spacing. Both the packed sand and dry mortar backstops were subject to out-of-sequence thrusting and basal erosion for an open subduction window (Fig. 5).

The spacing of frontal thrust faults was compiled for eight 'accretionary' and two 'non-accretionary' low basal friction experiments. When fault spacing is plotted against layer thickness, a linear relationship is observed (Fig. 6). Only the non-accretionary experiments N5 and N7 deviate from this relationship. Thus, the aspect ratio (length to thickness ratio) of a freshly initiated, undeformed thrust slice is constant (= 3.3), for an 'accretionary' material balance. This confirms the principle of self-similar wedge growth predicted by critical wedge theory. Furthermore, Mohr–Coulomb wedge theory (Davis *et al.*, 1983; Dahlen, 1984) also accurately predicts the taper of low basal friction experiments, with constant material addition at the wedge front.

In contrast to the pronounced frontal accretion and regular fault spacing common to all low basal friction experiments, high basal friction experiments are generally marked by: (1) a steeper surface slope, (2) wider fault spacing and (3) periods of underthrusting of the entire sedimentary section causing frontal erosion and retreat of the deformation front. This is illustrated in experiment N6 (Fig. 7a), where sustained underthrusting and subduction of the entire sedimentary section has caused substantial frontal erosion leading to an oversteepening of the toe, a trenchward tilt of the entire wedge and the formation of normal faults upslope.

For a positive, 'accretionary' mass balance, periods of frontal accretion alternate with underthrusting episodes leading to a cyclical variation in surface slope and fault spacing (Gutscher *et al.*, 1996). This is well illustrated in

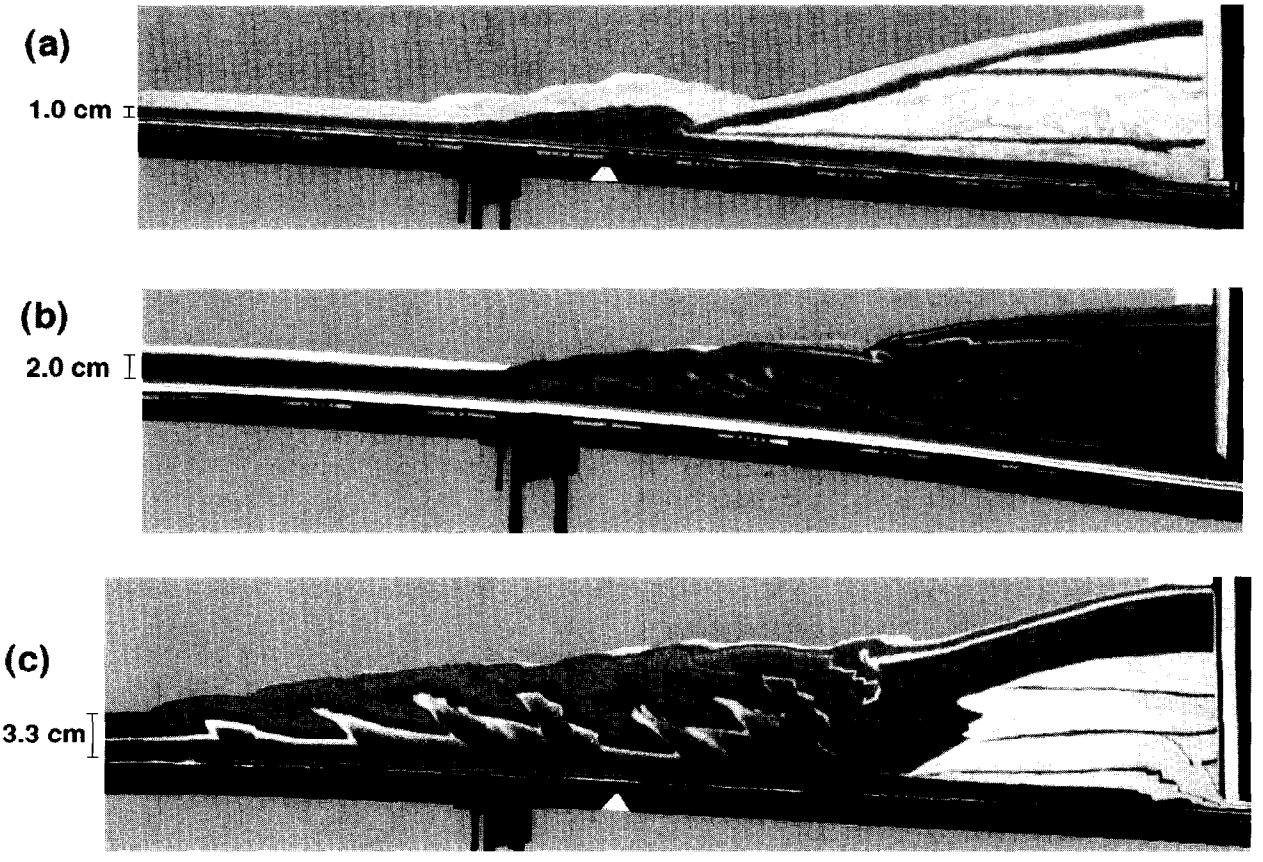

Fig. 5. Photographs of three low basal friction experiments with different layer thicknesses after the same amount of scaled convergence (20 × layer thickness). A similar number of regularly spaced thrust slices have formed at a shallow surface angle, confirming the principle of self-similar wedge growth. (All photos at same scale.) (a) Experiment N23f, Input = 1 cm, dry mortar backstop, initial $\alpha = 10°$, eight thrusts after 20 cm. (b) Experiment N4, Input = 2 cm, packed sand backstop, initial $\alpha = 6°$, after 40 cm. Here only six thrust slices have formed due to over 5 cm displacement along the out-of-sequence thrust. (c) Experiment N22, Input = 3.3 cm, dry mortar backstop, initial $\alpha = 15°$, seven thrusts after 65 cm.

experiment N18 (Fig. 7b) where a short thrust slice has just formed at the front after a 50 cm long sheet has been underthrust beneath the backstop. In this experiment an extra long (70 cm) backstop was used in order to test the maximum length of underthrust sheets and to eliminate any possible effects of the subduction window. Again, in contrast to their low basal friction counterparts, the initial surface slope of the backstop was observed to play a primary role in determining the phase of the accretionary cycle (Gutscher *et al.*, in press).

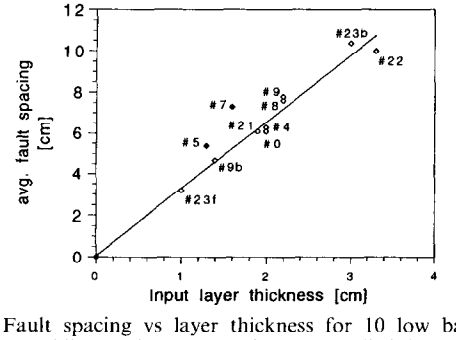

Fig. 6. Fault spacing vs layer thickness for 10 low basal friction experiments. All accretionary experiments (unfilled diamonds) obey a linear relation, confirming the principle of self-similar wedge growth.

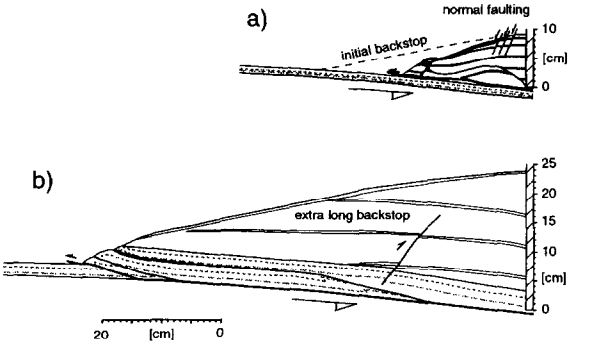

Fig. 7. Tectonic interpretation of two high basal friction experiments; (a) experiment N6, **Input** = 1.3 cm, **Output** = 2.0 cm, after 100 cm convergence. Note the steep scarp due to frontal erosion and the development of normal faults at the rear of the wedge. (b) experiment N18, **Input** = 2.0 cm, **Output** = 0.4 cm, after 60 cm convergence. Note the long, undeformed sheet underthrust beneath the wedge, followed by the formation of a shorter thrust slice.

Table 1. Physical parameters of the sand, other materials and basal surfaces

Material	Sand (sprinkled)	Sand (packed)	Dry mortar (packed)
Density (ρ)	1690 kg/m^3	1900 kg/m^3	2000 kg/m^3
Internal friction (μ_{int})	0.57	0.57	0.60
Cohesion (C_0)	20 Pa	100 Pa	150 Pa

low basal friction (polished PVC -sand) $\mu_b = 0.33$.
high basal friction (double sided adhesive tape sand) $\mu_b \approx 0.50$.

SUMMARY OF EXPERIMENTAL OBSERVATIONS

The experiments discussed above have shown that low basal friction produces long, narrow tapered wedges through continuous frontal accretion of imbricate thrust slices. Simultaneously, substantial basal erosion can occur, with little influence on the frontal dynamics. This is true for all cases; **I > O**, **I = O** and **I < O**, whereby the net growth or erosion of the wedge varies accordingly. The erosional (**I < O**) experiment N5, had the steepest final slope ($\alpha = 18°$), while the accretionary (**I > O**) experiments N0 and N4 had the shallowest final slope ($\alpha = 6$–$7°$). Minor to moderate underplating is observed in the cases **I ≥ O**. Backthrusting in the backstop wedge occurs in all three cases, but is most pronounced for the accretionary case (**I > O**). An outer arc high and accompanying forearc basin are then commonly produced. However, these are transient features in cases with subducted output. Spacing of frontal thrust faults for low basal friction is proportional to layer thickness for accretionary conditions. For high basal friction thrust fault spacing is variable though generally greater than for low basal friction. Underthrusting of the entire sedimentary section with associated frontal erosion is common. The theoretical basis for this mechanical difference is discussed elsewhere (Gutscher *et al.*, in press).

MATERIAL TRANSFER

A volumetric analysis of the six key experiments, plus six additional experiments covering a wider range of Input to Output ratios, was performed to determine the primary mode of material transfer for different initial boundary conditions. The following types of material transfer were quantified: (1) frontal accretion, (2) underthrusting and basal underplating, (3) subduction out of the system, (these three in terms of total input) and (4) basal erosion (of the initial backstop) as a fraction of the subducted sediment output. The objective is to relate these results to the initial conditions (i.e. basal friction and Input/Output ratio) and determine the relative importance of each tectonic process (Table 1).

Total input is the product of the sediment thickness times the sum of total convergence plus the advance (or retreat) of the deformation front. Thus, for a thickness of 2 cm and 100 cm convergence, with a 20 cm advance of the deformation front, the total input would be 240 cm^3 per cm length of 'trench'. Observed frontally accreted or basally underplated areas are measured from the final experimental section and expressed as a fraction of total input. Underplated material is defined as material transported beneath the backstop, but now located above the active detachment and thus no longer entrained towards the subduction window.

Material transfer is shown to depend strongly upon the basal friction (Fig. 8). In all low basal friction experiments (Fig. 8a), frontal accretion predominates and very little to no underplating occurs for the complete range of Input/Output ratios. In sharp contrast, the primary mode of wedge growth in high basal friction experiments (Fig. 8b) is underplating, which on average comprises from two to three times the amount of material accreted frontally or ca. 60% of the excess material input. Deviations from the sum of 100% are due to erosion of the backstop, additional 'Input' due to advance of the deformation front and minor (≤3%) errors in the measurement of the areas.

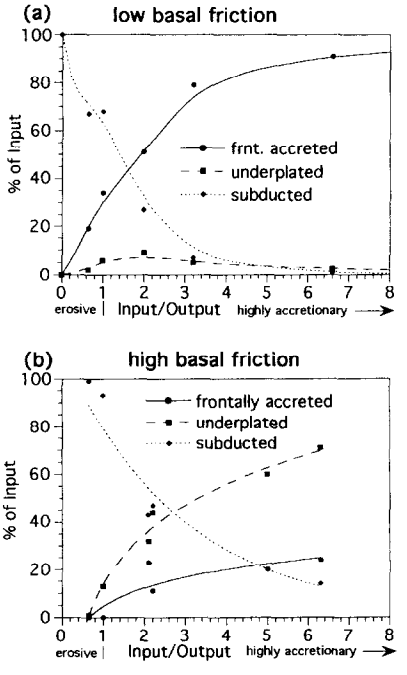

Fig. 8. Frontally accreted, basally underplated and subducted fractions as a function of **I/O** ratio; (a) for low basal friction experiments, (b) for high basal friction experiments, as a proportion of total available input.

Within the class of low basal friction experiments as a whole (Fig. 8a), there is an increase towards 100% frontal accretion for increasing Input/Output ratios, e.g. as the Output approaches zero, then 100% of the Input is accreted frontally by imbricate thrusting (e.g. experiment N0). More generally, when the ratio **I/O** > 1 (net wedge growth), then 40–90% of the available Input is accreted frontally. Underplating only plays a minor role, with a maximum of 5–10% of Input for Input/Output ratios of 1–3.

The fraction of material eroded from the base of the pre-existing wedge or backstop was also examined as a function of the two primary parameters, basal friction and Input/Output ratio. Here, total output is the product of convergence times the height of the output window. This output consists of material accreted at the front, then transported within the subduction channel and material removed from the backstop. The difference in the area of the backstop between the initial and final stages was used to determine this 'basally eroded fraction'.

The basally eroded fraction again reveals a pronounced difference between low and high basal friction. For low basal friction experiments with Output, a substantial portion (30–90%) of the material transported out of the system is derived from the backstop (Fig. 9). Whereas erosion of the backstop also occurs in non-accretionary (**I/O**≤1), high basal friction experiments, the material is removed primarily at the front, through mass wasting. All accretionary (**I/O** > 1), high basal friction experiments show practically no erosion at the base of the backstop (Fig. 9).

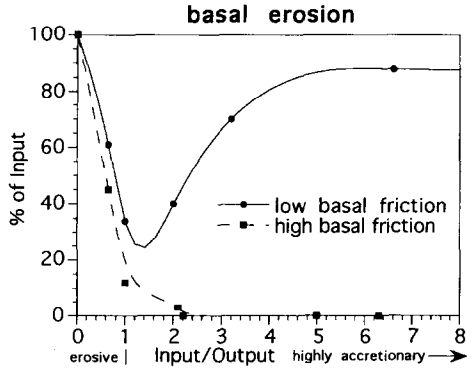

Fig. 9. Basal erosional fraction as a function of **I/O** ratio; for low and high basal friction experiments as a proportion of total output.

APPLICATION OF MODELS TO CONVERGENT MARGINS

The classification of different experimentally observed structural configurations according to the genetic conditions (basal friction, material balance) allows predictions to be made regarding the material parameters and material transfer in convergent margins. Some caution is necessary in applying the experimental observations to submarine accretionary wedges, however, since the analog experiments are performed with a dry, homogeneous material representing the accreting sediments. Granular materials typically used in the laboratory (e.g. sand) have an angle of repose of ca. 30°, steeper than commonly observed surface angles (α) in submarine sediments. In actual convergent margins, the effects of elevated pore pressure, as porous underconsolidated sediments are dewatered, can locally greatly weaken the sediments and produce important variations in material properties (Hubbert and Rubey, 1959; Bray and Karig, 1985; Moore, 1989; Byrne and Fisher, 1990). These cannot be reproduced directly, but must be simulated with different basal surfaces or different materials. However, two groups of observations indicate that the modeling results are indeed applicable to accretionary wedges. First, the surface angles from accretionary wedges around the world also exhibit a very wide spread (from 0.5° to over 20°) (Lallemand *et al.*, 1994) as do the range of slopes from analog experiments. Second, the well resolved structures (conjugate fore- and backthrusts, short, regularly spaced imbricate slices) seen in seismic profiles at the toe of some accretionary wedges, in particular the Nankai trough (fig. 10, Moore *et al.*, 1990) bear a striking resemblance to structures observed in sandbox experiments.

The problem of pore fluid pressure and its influence on material strength is best addressed using numerical methods. These allow a calculation of variations in fluid pressure throughout the wedge and indicate that these are dependent on, among other factors, wedge geometry

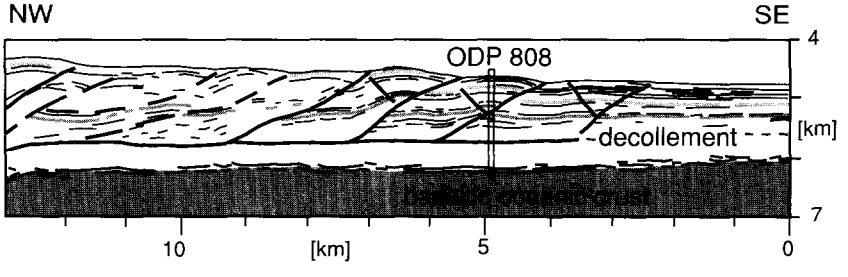

Fig. 10. Line drawing of the frontal portion of seismic reflection profile NT62-8 from the Nankai Trough (after Moore *et al.*, 1990). (Depth section, VE = 1.) Additional structural control is provided by ODP drill site 808.

Table 2. Total input, output andf accretionary fraction for six high μ_b and six low μ_b experiments (upper entries are experimental parameters, lower entries interpreted results)

	Low μ_b						High μ_b					
experiment	N5	N7	N4	N21	N22	N0	N6	N3	N1	N17	N18	N16
I/O	0.65	1.0	2.0	3.3	6.6	20	0.65	1.0	2.1	2.2	5.0	6.3
Input [cm]	1.3	1.6	2.0	2.0	3.3	2.0	1.3	1.6	2.1	1.5	2.0	2.0
Output [cm]	2.0	1.6	1.0	0.6	0.5	≤0.1	2.0	1.6	1.0	0.7	0.4	0.3
converg. [cm]	135	175	150	55*	80*	80*	145	180	140	175	100	165
$input_{tot}$ [cm^2]	156	272	332	152	219	396	162	272	318	262	200	354
$output_{tot}$ [cm^2]	270	280	150	40	33	8	290	288	140	122	40	50
frnt. accr. [cm^2]	30	93	170	120	360	219	0	0	73	30	40	85
underpl. [cm^2]	3	17	30	7	10	0	2	36	102	115	120	250
bas. eros. [cm^2]	165	96	60	35	23	8	130	34	4	0	0	0
frnt. accr. %	19	34	51	79	91	100	0	0	23	11	20	24
underpl. %	2	6	9	5	2	0	1	13	32	44	60	71
bas. eros. %	61	34	40	70	88	100	45	12	3	0	0	0

* = intermediate stage of experiment.

(Kukowski and Schillhorn, 1996). These fluid pressures can then be applied in complex models to calculate material strength and determine the location of deformation during subsequent shortening (Wang and Davis, submitted).

Three common accretionary configurations observed in the analog experiments are illustrated schematically (Fig. 11). For low basal friction, there is a frontal region of imbricate thrust slices with a shallow surface slope (α). For a small degree of basal erosion, an outer arc high develops bounded arcwards by a major backthrust (Fig. 11a). This corresponds to the configuration at the northern Colombian convergent margin (Ladd and Truchan, 1983) and to the overall geometry of the Barbados Ridge accretionary complex (Westbrook *et al.*, 1988). The southward increase in the sedimentary layer thickness in the Barbados Ridge complex (from 0.7 to 6 km) correlates to a linear increase in fault spacing (Mascle *et al.*, 1990), similar to the experimentally determined relation (Fig. 6).

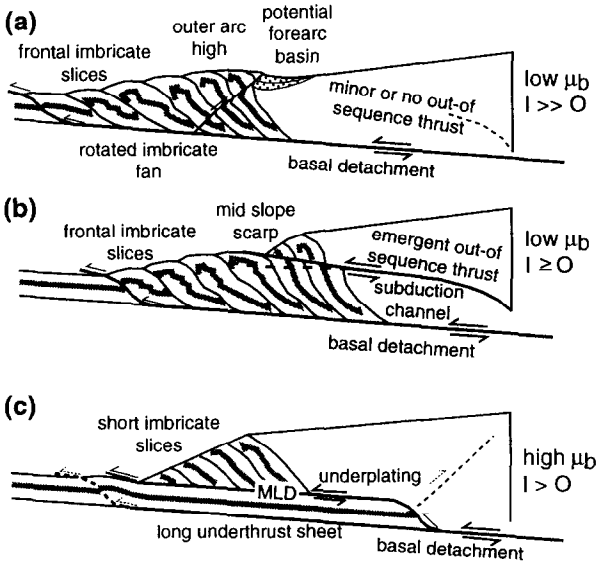

Fig. 11. Accretionary structural configurations and genetic boundary conditions. (a) Classic leading imbricate fan, with rotation of older thrust slices and one major backthrust producing an outer arc high. Observed for low basal friction and Input ≫ Output. (b) Imbricate fan, with emergent out-of-sequence thrust causing a mid-slope erosional scarp and bounding a subduction channel carrying partial and complete fault slices below the wedge. Observed for low basal friction and Input equal or slightly greater than Output. (c) Truncated imbricate fan, eroded by mass wasting along the steep frontal surface and cut below by the roof thrust of a long underthrusting sheet. MLD = mid-level detachment.

For substantial basal erosion, an emergent out-of-sequence thrust produces an erosional scarp at the mid-slope (Fig. 11b). This description may apply to the Nankai accretionary wedge (Aoki *et al.*, 1982). In line NT62-8 (Fig. 10), the frontal region has regularly spaced imbricate thrust slices and a very shallow slope (1–2°) implying low basal friction. Thirty-four kilometers arcwards from the deformation front there is a 12° scarp (Moore *et al.*, 1990), but the complex tectonic structure at depth and arcwards is poorly imaged. The frontal configuration alone, however, does not indicate whether the total mass balance is slightly positive or slightly negative, since frontal accretion of imbricate slices can occur in both cases. Independent data on wedge advance or wedge retreat (e.g. subsidence or uplift of the shelf and slope) are necessary. For comparison, a typical high basal friction configuration is shown (Fig. 11c) where both narrowly spaced imbricate slices and long sheets can develop (Gutscher *et al.*, 1996) (see also Fig. 7b). The wedge front can steepen up to ca. 30° through mass wasting associated with episodes of underthrusting. This can cause backthrust deformation in the backstop and lead to underplating. A high degree of structural diversity and corresponding frontal configurations are observed at the Alaska accretionary wedge (Gutscher *et al.*, in press).

Two commonly observed erosional configurations are presented below (Fig. 12). The low basal friction case also shows accretionary structures at the deformation front where imbricate thrust slices develop. These, however, are entrained as duplexes into the subduction channel and are subsequently completely eroded by basal or 'tectonic' erosion (Scholl *et al.*, 1980). Where the out-of-

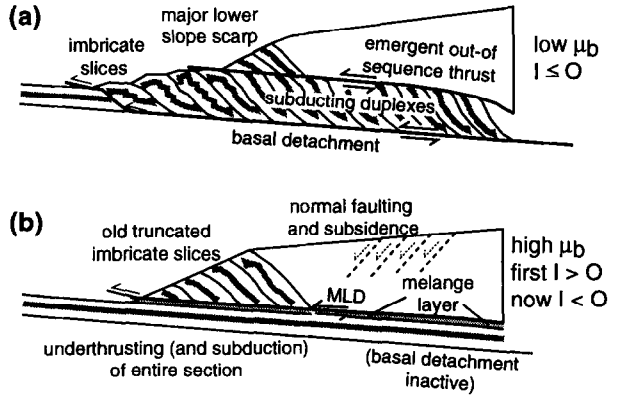

Fig. 12. Erosional structural configurations and genetic boundary conditions. (a) Low basal friction with emergent out-of-sequence thrust causing a major lower slope scarp and subduction of the imbricate slices as entrained duplexes. (b) High basal friction featuring underthrusting of the entire undeformed section, a steep frontal slope eroding older units and an entrained melange layer. Erosion causes collapse and rotation of the wedge forming normal faults.

sequence thrust emerges at the lower slope, a steep erosional scarp forms. These structural elements are observed in the Japan trench (von Huene *et al.*, 1994). Here, a frontal region of imbricate thrusting with a shallow surface slope (4–6°) is bounded by a ca. 20° scarp 5–10 km from the deformation front.

A steep erosional front and normal faults above the lower slope are characteristic features of the erosional high basal friction case (Fig. 12b). In the Mariana Trench such a configuration is observed (Hussong and Uyeda, 1982). In the Southern Kuril Trench, the frontal slope is moderate (4–6°), but normal faulting upslope has been reported (Klaeschen *et al.*, 1994). The moderate frontal slope may be the product of renewed accretion or of offscraping of a small portion of the trench sequence similar to that reported in Costa Rica (Shipley *et al.*, 1992). Here too, normal faulting is observed upslope (McIntosh *et al.*, 1993).

CONCLUSIONS

The series of analog experiments reported here allowed the material transfer to be quantified for systematically controlled boundary conditions.

— For low basal friction, material transfer during wedge growth occurs almost exclusively by frontal accretion of imbricate thrust slices. Substantial basal erosion occurs for an open subduction window, simultaneously with frontal accretion.

— For high basal friction, the dominant mode of material transfer during wedge growth is underplating. Frontal erosion occurs during underthrusting episodes.

Thrust fault spacing was found to be affected by basal friction.

— For low basal friction and an accretionary material balance, fault spacing is proportional to layer thickness confirming the principal of self-similar wedge growth.

— For high basal friction, thrust spacing is variable, though generally greater.

Applying the results of the systematic experimental investigation to convergent margin configurations, one can infer that wide, shallow dipping wedges, with a pronounced outer arc high and with short, regularly spaced imbricate thrusts, like the northern Colombia margin, or southern Barbados Ridge complex, have a low basal friction and excess material input.

On the other hand, slope breaks or scarps, like in the Japan Trench and Nankai Trough, imply out-of-sequence thrusting and basal erosion (low basal friction with output), or alternatively, arcward variations in material properties.

The models discussed above illustrate one of the strengths of sandbox experiments: the ability to follow the evolution of complex structures through time. They suggest that in accretionary wedges episodic, transient and progressive deformation processes can occur, despite constant material properties and mass transfer boundary conditions.

Acknowledgements—Experiments were performed at the Laboratoire de Géophysique et Tectonique, CNRS—UMR 5573, ISTEEM, Univ. Montpellier II and the costs met by the Centre National de la Recherche Scientifique. Funding was provided by the Deutsche Forschungsgemeinschaft (Project Ku1000/1) and travel expenses were met by Procope.We thank Roland von Huene, Dirk Kläschen, Jürgen Frühn, Bernard Sanche and Stephane Dominguez for fruitful discussions, access to valuable seismic reflection data and technical assistance in the laboratory. We also thank Julia Morgan and an anonymous reviewer for constructive remarks which helped improve the original manuscript.

REFERENCES

Aoki, Y., Tamano, T. and Kato, S. (1982) Detailed structure of the Nankai Trough from migrated seismic sections. In: *Studies in continental margin geology, American Association of Petroleum Geologists—Memoir*, eds J. S. Watkins and L. L. Drake, **34**, 309–322.

Bray, C. J. and Karig, D. E. (1985) Porosity of sediments in accretionary prisms and some implications for dewatering processes. *Journal of Geophysical Research* **90**, 768–778.

Byrne, D., Davis, D. and Sykes, L. (1988) Loci and maximum size of thrust earthquakes and the mechanics of the shallow region of subduction zones. *Tectonics* **7**, 833–857.

Byrne, D., Wang, W. and Davis, D. (1993) Mechanical role of backstops in the growth of forearcs. *Tectonics* **12**, 123–144.

Byrne, T. and Fisher, D. (1990) Evidence for a weak and overpressured décollement beneath sediment-dominated accretionary prisms. *Journal of Geophysical Research* **95**, 9081–9097.

Dahlen, F. (1984) Noncohesive critical Coulomb wedges: An exact solution. *Journal of Geophysical Research* **89**, 10125–10133.

Davis, D., Suppe, J. and Dahlen, F. (1983) Mechanics of fold and thrust belts and accretionary wedges. *Journal of Geophysical Research* **88**, 1153–1172.

Davis, E. E., Hyndman, R. D. and Villinger, H. (1990) Rates of fluid expulsion from the Northern Cascadia accretionary prism: constraints from new heat flow and multichannel seismic reflection data. *Journal of Geophysical Research* **95**, 8869–8889.

Dickinson, W. R. and Seely, D. R. (1979) Structure and stratigraphy of forearc regions. *American Association of Petroleum Geologists Bulletin* **63**, 2–31.

Gutscher, M.-A., Kukowski, N., Malavieille, J. and Lallemand, S. (1996) Cyclical behavior of thrust wedges: insights from high basal friction sandbox experiments. *Geology* **24**, 135–138.

Hoshino, K., Koide, H., Inami, K., Iwamura, S. and Mitsui, S. (1972) Mechanical properties of Japanese Tertiary sedimentary rocks under high confining pressures. *Report 244, Geological Survey of Japan*. Kawasaki, pp. 200.

Hubbert, M. L. and Rubey, W. W. (1959) Role of fluid pressure in mechanics of overthrust faulting. *Bulletin of the Geological Society of America* **70**, 115–206.

Hussong, D. M., Rees, T. B. and Bartlett, W. A. (1988) SeaMARC II sonar imagery and bathymetry of the Nazca Plate and Peru Forearc, Ocean Drilling Program leg 112. In: *Proceedings of the Ocean Drilling Program, Initial Reports*, ed. E. Suess, R. v. Huene *et al.*, pp. 125–130. College Station, Texas A112.

Hussong, D. M. and Uyeda, S. (1982) *Proceedings of the Deep Sea Drilling Project, Initial Reports* Washington, D.C., U.S. Government Printing Office, 60.

Klaeschen, D., Belykh, I., Gnibidenko, H., Patrikeyev, S. and von Huene, R. (1994) Structure of the Kuril Trench from seismic reflection records. *Journal of Geophysical Research* **99**, 24173–24188.

Kukowski, N., von Huene, R., Malavieille, J. and Lallemand, S. (1994) Sediment accretion against a buttress beneath the Peruvian continental margin as simulated with sandbox modelling. *Geologische Rundschau* **83**, 822–831.

Kukowski, N. and Schillhorn, T. (1996) Modeling of fully coupled transient fluid and heat transport in growing accretionary wedges. *EOS* **77**(46), 701.

Ladd, J. W. and Truchan, M. (1983) Compressional features across the Caribbean Margin of Columbia. In: *Seismic Expression of Structural Style, American Association of Petroleum Geologists—Studies in Geology*, ed. A. W. Bally, pp. 163–166. series N15, 3, American Association of Petroleum Geologists, Tulsa Oklahoma.

Lallemand, S. (1992a) Transfert de matière en zone de subduction (Material Transfer in Subduction Zones) Travaux publiés depuis (1990), **1**, 189.

Lallemand, S. (1992b) Réflexions sur les conséquences de l'erosion tectonique, **2**, 96. Habilitation Thesis, *Memoires des Sciences de la Terre*, Université Pierre et Marie Curie, Paris, 92 – 97.

Lallemand, S., Schnürle, P. and Malavieille, J. (1994) Coulomb theory applied to accretionary and nonaccretionary wedges: Possible causes for tectonic erosion and/or frontal accretion. *Journal of Geophysical Research* **99**, 12033–12055.

Larroque, C., Calassou, S., Malavieille, J. and Chanier, F. (1995) Experimental modelling of forearc basin development during accretionary wedge growth. *Basin Research* **7**, 255–268.

Leeman, W. P., Carr, M. J. and Morris, J. D. (1994) Boron geochemistry of the Central American Arc: Constraints on the genesis of subduction-related magmas. *Geochemica et Cosmochemica Acta* **58**, 149–168.

Liu, H., McClay, K. R. and Powell, D. (1992) Physical models of thrust wedges. In: *Thrust Tectonics*, ed. K. R. McClay, pp. 71–81. London, Chapman and Hall.

Malavieille, J. (1984) Modélisation expérimentale des chevauchements imbriqués: application aux chaines de montagnes. *Bulletin de la Societé Géolgique Francaise* **7**, 129–138.

Malavieille, J., Calassou, S., Larroque, C., Lallemand, S. and Stephan, J. F. (1991) Modélisation analogique des prismes d'accrétion océaniques. *Video Presentation 27th Course Series M037*, (french and english versions) Exploration Studies, Elf Aquitaine.

Malavieille, J., Calassou, S. and Larroque, C. (1993) Modélisation expérimentale des relations tectonique sedimentation entre bassin avant-arc et prisme d'accretion. *Comptes Rendu à l'Academie des Sciences* **316**, 1131–1137.

McIntosh, K. D., Silver, E. A. and Shipley, T. H. (1993) Evidence and mechanisms for forearc extension at the accretionary Costa Rica convergent margin. *Tectonics* **12**, 1380–1392.

Moore, G. F., Shipley, T., Stoffa, P., Karig, D., Taira, A., Kuramoto, S., Tokuyama, H. and Suyehiro, K. (1990) Structure of the Nankai Trough accretionary zone from multichannel seismic reflection data. *Journal of Geophysical Research* **95**, 8753–8765.

Moore, J. C. (1989) Tectonics and hydrogeology of accretionary prisms: role of the décollement zone. *Journal of Structural Geology* **11**, 95–106.

Moore, J. C., Diebold, J., Fisher, M. A., Sample, J., Brocher, T., Talwani, M., Ewing, J., von Huene, R., Rowe, C., Stone, D., Stevens, C. and Sawyer, D. (1991) EDGE deep seismic reflection transect of the eastern Aleutian arc-trench layered lower crust reveals underplating and continental growth. *Geology* **19**, 420–424.

Moore, J. C., Shipley, T. H. and 26 others (1995) Abnormal fluid pressures and fault-zone dilation in the Barbados accretionary prism: Evidence from logging while drilling. *Geology* **23**, 605–608.

Morris, J. D., Leeman, W. P. and Tera, F. (1990) The subducted component in island arc lavas: constraints from Be isotopes and B–Be systematics. *Nature* **344**, 31–36.

Mulugeta, G. (1988) Modelling the geometry of Coulomb thrust wedges. *Journal of Structural Geology* **10**, 847–859.

Pacheco, J. F., Sykes, L. R. and Scholz, C. H. (1993) Nature of seismic coupling along simple plate boundaries of the subducting type. *Journal of Geophysical Research* **98**, 14133–14159.

Scholl, D. W., von Huene, R., Vallier, T. L. and Howell, D. G. (1980) Sedimentary masses and concepts about tectonic processes at underthrust ocean margins. *Geology* **8**, 564–568.

Shipley, T., McIntosh, K., Silver, E. and Stoffa, P. (1992) Three-dimensional seismic imaging of the Costa Rica accretionary prism: structural diversity in a small volume of the lower slope. *Journal of Geophysical Research* **97**, 4439–4459.

Taira, A., Hill, I., Firth, J., Berner, U., Brückmann, W., Byrne, T., Chabernaud, T., Fisher, A., Foucher, J. P., Gamo, T., Gieskes, R., Hyndman, R., Karig, D., Kastner, M., Kato, Y. and Lallemant, S. (1992) Sediment deformation and hydrogeology of the Nankai Trough accretionary prism: Synthesis of shipboard results of Ocean Drilling Program Leg 131. *Earth and Planetary Science Letters* **109**, 431–450.

von Huene, R. and Lallemand, S. (1990) Tectonic erosion along the Japan and Peru convergent margins. *Bulletin of the Geological Society of America* **102**, 704–720.

von Huene, R. and Scholl, D. (1991) Observations at convergent margins concerning sediment subduction, subduction erosion and the growth of continental crust. *Reviews in Geophysics* **29**, 279–316.

von Huene, R., Klaeschen, D., Cropp, B. and Miller, J. (1994) Tectonic structure across the accretionary and erosional parts of the Japan Trench margin. *Journal of Geophysical Research* **99**, 22349–22361.

von Huene, R., Flueh, E., Cropp, B., Csernok, T., Fabel, E., Hoffmann, J., Emeis, K., Holler, P., Jeschke, G., Leandro, C., Perez-Fernandez, I., Chavarria, J., Florez, A., Escobedo, D., Leon, R. and Barrios, O. (1995) Morphotectonics of the Pacific convergent margin of Costa Rica. In: *Geologic and Tectonic Development of the Caribbean Plate Boundary in Southern Central America, Special Paper 295*, ed. P. Mann, pp. 291–307. Boulder, Colorodo, Geological Society of America.

von Huene, R., Pecher, I. and Gutscher, M.-A. (1996) Development of the accretionary prism along Peru and material flux after subduction of Nazca Ridge. *Tectonics* **15**, 19–33.

Wang, W.-H. and Davis, D. M. (1996) Sandbox model simulation of forearc evolution and non-critical wedges. *Journal of Geophysical Research* **101**, 11329–11339.

Westbrook, G. K., Smith, M. J., Peacock, J. H. and Poulter, M. J. (1982) Extensive underthrusting of undeformed sediment beneath the accretionary complex of the Lesser Antilles subduction zone. *Nature* **300**, 625–628.

Westbrook, G. K., Ladd, J. W., Buhl, P., Bangs, N. and Tiley, G. J. (1988) Cross section of an accretionary wedge: Barbados Ridge complex. *Geology* **16**, 631–635.